Publ. Astron. Soc. Japan 39, 309–327 (1987)

Transonic Disk Accretion Revisited

Jun FUKUE

Astronomical Institute, Osaka Kyoiku University, Tennoji-ku, Osaka 543

(Received 1986 July 14; accepted 1986 October 4)

Abstract

Disk accretion of ideal gas with angular momentum is examined under a full relativistic treatment. The rigorous equations of state are used in order to deal properly with the relativistic flow. There appear multiple critical points in some ranges of parameters similar to the polytropic flow. A transition through standing shocks is also examined in relation to the accretion onto a compact star. It is found that for the same parameters and boundary conditions the positions of standing shocks multiply like critical points due to the rotation and relativistic effects. An application to low-mass binary X-ray sources is briefly discussed. In these objects, the very cold transonic flow inside the inner edge of the accretion disk may form the hot atmosphere around a neutron star via shocks.

Key words: Accretion; Equations of state; Standing shock waves; Transonic flows; X-ray binaries.

1. Introduction

Recent observational developments around neutron stars and black holes require a deeper study of an accretion of gas with angular momentum onto such compact objects. Although there are a number of works on accretion disk models, it has been assumed in almost all cases a Keplerian disk where the radial drift velocity is neglected and the gravitational attraction of a central object is balanced by rotation (Shakura and Sunyaev 1973; Novikov and Thorne 1973). However, in the region between the inner edge of an accretion disk and the surface of the central object (figure 1b), an initially subsonic flow becomes supersonic through a critical point, as well as in the case where the infalling gas is originally unbound and has a small angular momentum (figure 1a). An accretion flow through a sonic point may be also established inside the cusp of a geometrically thick disk—an accretion torus (figure 1c) (Kozłowsky et al. 1978; Rees et al. 1982). In this paper, I generally examine such a transonic flow onto compact objects in the framework of general relativity.

To date, accretion and wind of gas with angular momentum have been investigated in the Newtonian case (Limber 1967; Henriksen and Heaton 1975) and in the relativistic case (Liang and Thompson 1980; Abramowicz and Zurek 1981; Loska 1982; Muchotrzeb 1983; Matsumoto et al. 1984; Lu 1985). When the accreting gas has angular momentum, center-type critical points appear in addition to usual saddle-

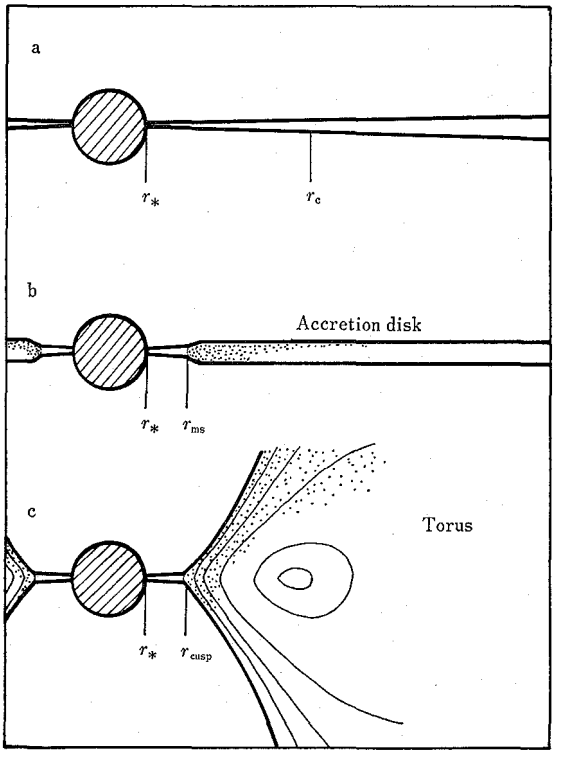

Fig. 1. Schematic pictures of several situations where a transonic disk accretion takes place. (a) The case where the accreting gas is unbound and initially has small angular momentum. The flow which becomes transonic at r_c reaches the surface r_* of a central object with or without shocks. (b) The case where a geometrically thin viscous accretion disk exists and the radius r_* is smaller than the marginally stable radius r_{ms}. In this case, a transonic flow is established in the region between r_{ms} and r_*. (c) The case where a geometrically thick disk—a torus—is formed. The gas overflowing the cusp at r_{cusp} accretes transonically to a central object.

type critical points in spherical flows. In the relativistic case, furthermore, another saddle-type point can exist and the bimodal behavior of accretion due to the jump between the inner critical point and the outer one was suggested (Abramowicz and Zurek 1981; Abramowicz et al. 1986). If the viscous process is relevant, the characteristic of the flow becomes more complicated (Matsumoto et al. 1984).

The present study is different from the previous investigations in three major aspects. First, the nature of transonic flows of rotating gas has been investigated in wide ranges of parameters in the present analysis, while the attentions were focused on several special cases in the previous studies. The second distinct point here is the adoption of the rigorous equations of state. The polytropic relation was assumed so far for simplicity. In an accretion onto a relativistic object, however, the relevant temperature range is very wide from the nonrelativistic regime to the relativistic regime. Hence the assumption of constant polytropic index is inadequate. Instead, we must use the equations of state for the relativistic Maxwell–Boltzmann gas (Fukue

1986). Finally, standing shock waves in transonic accreting flows are also considered in this work. A transition of a supersonically accreting flow to a subsonic one through standing shocks is important in the disk accretion onto a compact star which has a rigid surface as well as onto a black hole.

In the next section, the basic equations governing a transonic flow are presented. Critical points of the system of the basic equations are obtained in section 3, whereas in section 4 critical solutions are classified on the parameter plane. Standing shocks are examined in section 5. Applications of the present flow to low-mass binary X-ray sources are made in section 6. The final section is devoted to conclusions. For convenience of the reader, the adiabatic sound speed and effective adiabatic index of the relativistic Maxwell–Boltzmann gas are given in appendix 1. The transonic disk accretion for the polytropic gas is summarized in appendix 2 in order to compare it with the present flow.

2. Basic Equations

Let us consider a steady axisymmetric disk accretion onto a compact star in the Schwarzschild space-time (figure 1). The flow is assumed to be one-dimensional in the radial (r) direction. The accreting gas, which consists of electrons and protons, is supposed to be adiabatic and inviscid. The magnetic field and self-gravity of the gas are both neglected for simplicity. Throughout this paper, we set r_g (the Schwarzschild radius)$=1=c$ (the light speed), unless otherwise mentioned. The subscripts e and p denote respectively electrons and protons.

Under these assumptions, the conservation of number density becomes

$$Anu^r=\text{constant}\,, \tag{1}$$

where A is the cross-sectional area of the flow and assumed to be proportional to r^N (to be explained later in this section). The total number density n is related to the proton number density n_p by $n=n_e+n_p=2n_p$. The radial component u^r of the four velocity is expressed as

$$u^r=\gamma v_r(g_{00})^{1/2}=\gamma_v v(g_{00})^{1/2}\,, \tag{2}$$

where γ is the Lorentz factor $\gamma=(1-v_r{}^2-v_\varphi{}^2)^{-1/2}=\gamma_v\gamma_L$; $\gamma_v\equiv(1-v^2)^{-1/2}$ and $\gamma_L\equiv(1-v_\varphi{}^2)^{-1/2}$. The physical radial and azimuthal velocities measured by the static observer are respectively $v_r=(-g_{rr}/g_{00})^{1/2}u^r/u^0$ and $v_\varphi=(-g_{\varphi\varphi}/g_{00})^{1/2}u^\varphi/u^0$, while the physical three-velocity measured by the corotating observer is $v=\gamma_L v_r$ (see Lu 1985). Finally, g_{ij}'s are metric tensors; e.g., $g_{00}=(1-1/r)$.

The relativistic Euler equation is

$$u^r\frac{du^r}{dr}+\frac{1}{2r^2}-\left(r-\frac{3}{2}\right)u^\varphi u^\varphi=-\left(1-\frac{1}{r}+u^r u^r\right)\frac{1}{\varepsilon+p}\frac{dp}{dr}\,, \tag{3}$$

where u^φ is the azimuthal component of the four velocity, and ε and p are the total internal energy density and the total pressure, respectively. The equation of angular momentum conservation is

$$u^r \frac{du^\varphi}{dr}+\frac{2u^r u^\varphi}{r}=-\frac{u^r u^\varphi}{\varepsilon+P}\frac{dp}{dr}\,. \tag{4}$$

By use of equation (1), the energy equation is written as

$$\frac{d\varepsilon}{dr}-\frac{\varepsilon+p}{n_p}\frac{dn_p}{dr}=0\,. \tag{5}$$

On the other hand, the total energy conservation along the flow stream line is given by an integrated form:

$$A(\varepsilon+p)u_0 u^r=\text{constant}\,, \tag{6}$$

where $u_0=\gamma(g_{00})^{1/2}$.

These equations are supplemented by equations of state:

$$p=nkT=2n_p kT\,, \tag{7}$$

$$\varepsilon=n_p f_p+n_e f_e=n_p(f_p+f_e)\,, \tag{8}$$

where k is the Boltzmann constant, T the common temperature of electrons and protons, and f_a's function of T (appendix 1).

The basic equations (1), (3)–(5), (7), and (8) determine the dynamical properties of the disk flow. It should be noted that the hydrostatic balance in the vertical direction of the disk is not treated in this paper for simplicity. Instead, it is assumed $A\propto r^N$, N being constant. Furthermore, N will be set to 2, since the qualitative properties are not much dependent on the values of N.

Dividing the total energy conservation (6) by the baryon number density conservation (1), we have the relativistic Bernoulli equation:

$$(f_p+f_e+2kT)u_0=\text{constant}=(m_p+m_e)E\,, \tag{9}$$

where E is the specific energy of the flow measured at infinity and read as Ec^2 in a dimensional form. Here equations of state (7) and (8) are used.

With the help of equation (5), the equation of angular momentum conservation (4) is easily integrated to give

$$r^2 u^\varphi \frac{\varepsilon+p}{n_p}=\text{constant}\,. \tag{10}$$

From the Bernoulli equation (9), this equation (10) ultimately becomes

$$\frac{r^2 u^\varphi}{u_0}=\text{constant}=L\,, \tag{11}$$

where L is the specific angular momentum of the gas measured at infinity. At this stage, γ_L is written as $\gamma_L=(1-g_{00}L^2/r^2)^{-1/2}$.

Finally, the basic equations are reduced to the *wind equations* such as

$$\frac{dv}{dr}=\frac{(1-v^2)v\{c_s^2 N/r-(1-c_s^2)/(2r^2 g_{00})+\gamma_L^2[1-(3/2r)]L^2/r^3\}}{v^2-c_s^2} \tag{12}$$

or

$$\frac{dT}{dr}=\frac{2T/(f_p'+f_e')\{-v^2N/r+(1-v^2)/(2r^2g_{00})-\gamma_L^2[1-(3/2r)]L^2/r^3\}}{v^2-c_s^2}, \tag{13}$$

where

$$c_s^2=\left(1+\frac{2k}{f_p'+f_e'}\right)\frac{2kT}{f_p+f_e+2kT} \tag{14}$$

is the square of the adiabatic sound speed (appendix 1) and the prime denotes the differentiation with respect to T. Equations (12) and (13) are dependent on each other through the Bernoulli equation (9).

In the polytropic flow, an apparently similar equation [e.g., equation (12)] is obtained (appendix 2). However, the sound speed c_s differs in each case. In the present case adopting the rigorous equations of state, the adiabatic index is no longer the parameter but a function of T as well as c_s.

In what follows, equation (13) is used as a basic wind equation, T being the variable. Thus, the basic equations in the final form to be solved are equations (1), (7)–(9), (11), and (13). In addition, the parameters to be specified are the mass accretion rate, the geometrical parameter N, the specific energy E, and the specific angular momentum L.

3. Critical Points and Their Topology

As is easily seen, equation (13) [or equation (12)] has critical points where both the denominator and numerator vanish simultaneously. These critical conditions are written as

$$v^2|_c=c_s^2|_c=\left.\frac{[1/(2r^2g_{00})]-\{[1-(3/2r)](L^2/r^3)/(1-g_{00}L^2/r^2)\}}{(N/r)+(1/2r^2g_{00})}\right|_c, \tag{15}$$

where the subscript c denotes the quantities at critical points.

This equation (15), the Bernoulli equation (9), and the sound speed (14) evaluated at critical points yield the relations among the quantities at critical points. The relations among L, E, and r_c (the location of critical points) are shown in figure 2. The parameter N is fixed as $N=2$.

It is emphasized that there appear multiple (2 or 3) critical points for some range of values of L and E, similar to the polytropic case examined previously (e.g., Liang and Thompson 1980; Lu 1985). The relations among L, E, and r_c, however, are quantitatively different from those of the polytropic case (appendix 2). For example, there exist three critical points for $1<E<1.00871$ in the present case adopting the rigorous equations of state, whereas in the polytropic case with index $\Gamma=4/3$ there exist three for $1<E<1.0215$ (Lu 1985).

The parameter values allowed are restricted by several physical conditions such that γ_L^2 must be positive at critical points or v^2 must be also positive there. The former condition is written as $L^2<r^2/g_{00}|_c$, whereas the latter, $v^2|_c>0$, becomes

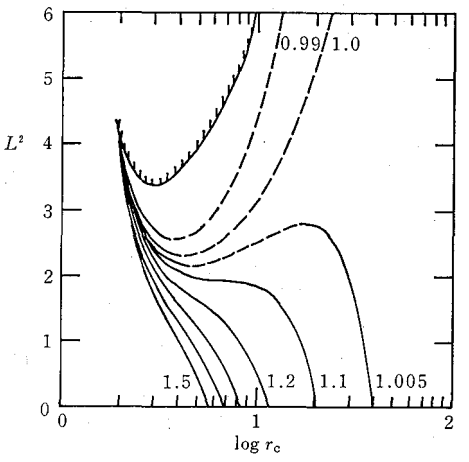

Fig. 2. The relations among L, E, and r_c. The abscissa is r_c and the ordinate is L^2. The number attached on each curve is the value of E (=0.99, 1.0, 1.005, 1.1–1.5). The parameter is $N=2$. It is noted that in some range of E there are multiple solutions r_c for a fixed L. Critical points are of the saddle type (denoted by solid curves) or of the center type (dashed curves). For the steady transonic flow, the values of parameters in the hatched region are forbidden because $v^2|_c<0$ there.

$$L^2<r/(2g_{00}{}^2)|_c\ , \tag{16}$$

which is the stronger condition than the former and also shown in figure 2. That is, the values of the parameters in the hatched region in figure 2 are forbidden because $v^2|_c<0$ there.

Also noted is the case of $E<1$. Because of the relativistic effect, the accretion from a bound orbit ($E<1$) is possible as described in figure 1b or 1c and will be discussed in section 6.

Linear expansions of the wind equation around critical points tell their topology. When there are three critical points, an intermediate point is not of spiral type as suggested previously (Lu 1985) but always of the *center type* (denoted by dashed curves in figure 2) as long as the adiabatic flow is relevant. The intermediate point becomes of the spiral type or of the nodal type when the viscous effect is taken into account (Matsumoto et al. 1984). On the other hand, inner and outer points are both saddles (denoted by solid curves in figure 2).

The reason for multiplicity is due to the existence of angular momentum and to the relativistic effect. When there are three critical points, an intermediate point of the center type is caused by the angular momentum of the gas like in the Newtonian case (Henriksen and Heaton 1975). On the other hand, the origin of the inner critical point is purely the relativistic effect (Liang and Thompson 1980).

4. Critical Solutions and Their Classification

As shown in the previous sections, when the geometrical parameter N, the specific energy of the flow (specific enthalpy at infinity for accretion) E, and the specific angular

momentum L are given, we can obtain the positions of critical points (figure 2) and further calculate critical solutions passing through critical points of the saddle type. In this section, I shall try to classify the critical solutions after presenting several typical solutions. For brevity, the geometrical parameter N is fixed as $N=2$.

4.1. Critical Solutions

Typical critical solutions are shown in figure 3 for parameters of $E=1.005$ and $L=1.500$, 1.522, and 1.600.

In figure 3, the Mach number M, the flow velocity v, the sound speed c_s, the flow temperature T, and the effective adiabatic index Γ are shown as functions of r. Thick curves represent accreting solutions, while thin curves show wind solutions.

In figure 3a ($L=1.500$), the critical solutions which extend from infinity to the surface of the central object pass through the outer critical point ($r_c=27.67$), although

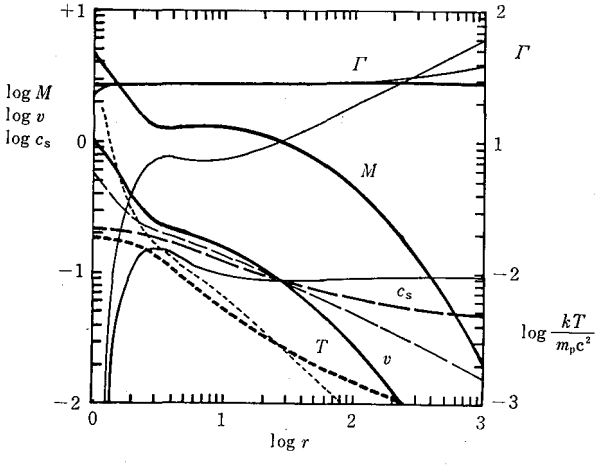

(a)

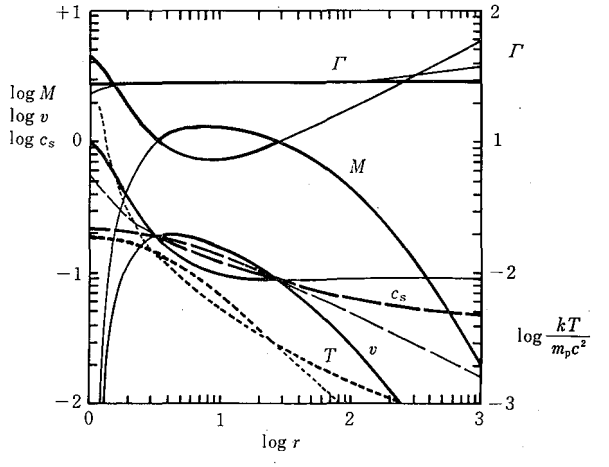

(b)

Fig. 3. See the caption on the next page.

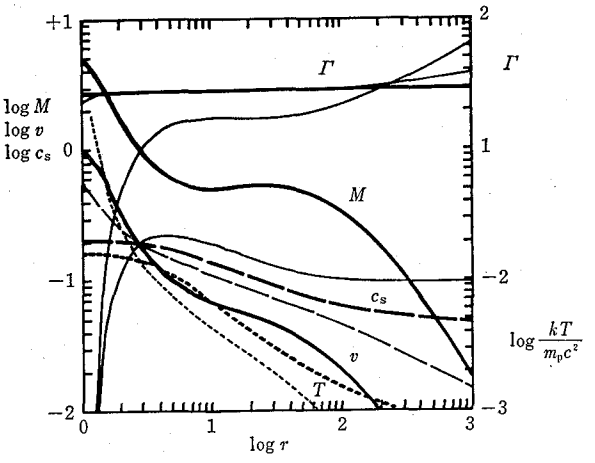

(c)

Fig. 3. The Mach number M, the flow velocity v, the sound speed c_s, the flow temperature T, and the effective adiabatic index Γ of typical critical solutions. The parameters are fixed as $N=2$, $E=1.005$, and $L=1.5$ (a), 1.522 (b), and 1.6 (c). Thick curves represent accreting solutions, while thin ones represent wind solutions. The critical solution passes through the outer critical point in (a), whereas it passes through the inner point in (c).

there exists an inner critical point of the saddle type at $r_c=3.55$. On the other hand, they pass through the inner one ($r_c=2.809$) in figure 3c ($L=1.600$), where the outer critical point is located at $r_c=24.17$. For special values of parameters, e.g., $L=1.522$ in the case of figure 3b, they pass through both inner and outer critical points of the saddle type ($r_c=3.31$ and 27.05 in this case). However, such a situation where particular values of parameters are selected will not be realized in actual flows.

The jump between the flow of the figure 3a type and that of the 3c type will take place through the 3b type as pointed out by Abramowicz et al. (1986) (see also subsection 4.2).

4.2. Classification

It is useful to classify solutions on the L-E parameter plane (figure 4). By means of the number of critical points appeared on the solution plane, the L-E plane is roughly divided into three regions:

(i) The region where there exist no critical solutions or no physical solutions which extend from infinity to the center (hatched region in figure 4). For the values of parameters in the lower-left region of figure 4, there are no critical points and thereby no critical solutions. On the other hand, in the rightward of the L-E plane, v^2 at inner critical points becomes negative (cf. figure 2), although there formally exist critical points. In this region, the high angular momentum of the flow prevents the gas to accrete steadily onto the central object (through inner critical points).

These two domains are merged at $L=L_{ms}=(27/8)^{1/2}=1.837$ and $E=E_{ms}=(8/9)^{1/2}=0.9428$. It should be noted that L_{ms} is not $3^{1/2}$ of a particle in the marginally stable last orbit, because the gas pressure is here taken into account (see Kozłowsky et al. 1978).

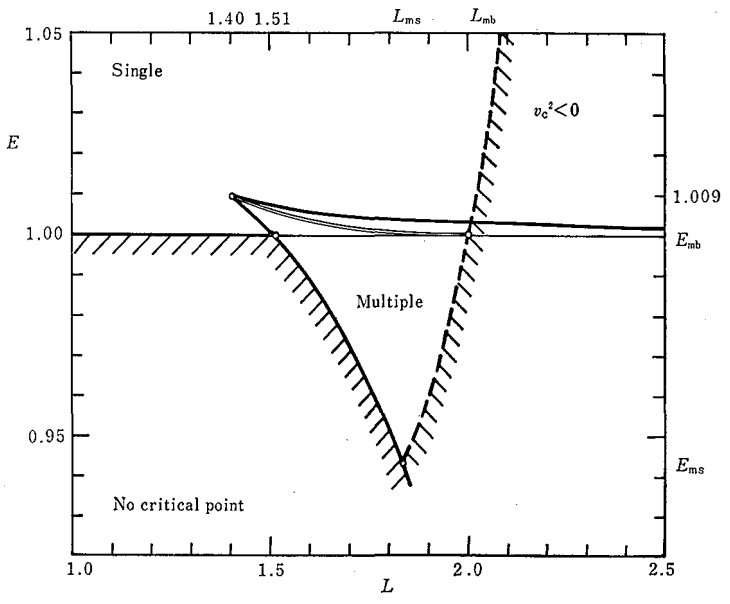

Fig. 4. The classification diagram on the L-E parameter plane. The plane is divided into three distinct regions via the number of critical points. The bifurcation points on the boundary of each domain are $(L, E, r_c)=(1.4047, 1.0087, 6.7)$, $(1.5151, E_{mb}, 4.3)$, $(L_{ms}, E_{ms}, 3)$, and $(L_{mb}, E_{mb}, 2)$, where $L_{ms}=(27/8)^{1/2}$, $L_{mb}=2$, $E_{ms}=(8/9)^{1/2}$, and $E_{mb}=1$. See the text for details.

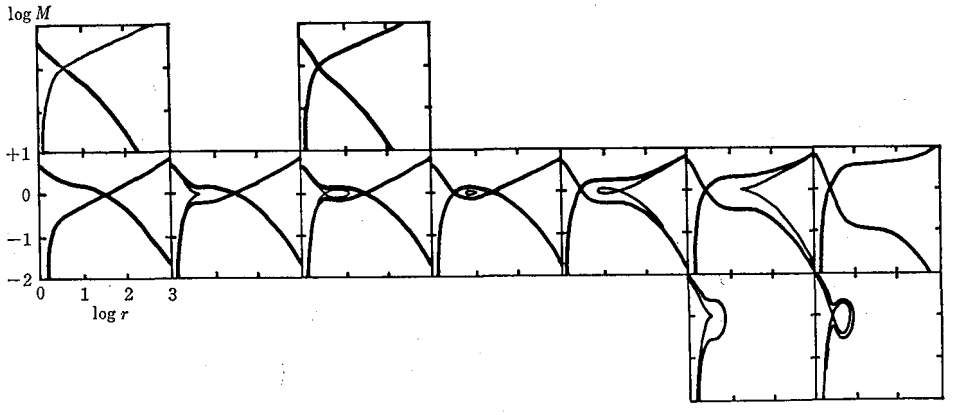

Fig. 5. The Mach numbers for several parameters in figure 4. From top-left to bottom-right, parameters are $(L, E)=(1.20, 1.04)$, $(1.50, 1.04)$, $(1.20, 1.005)$, $(1.46, 1.005)$, $(1.50, 1.005)$, $(1.52, 1.005)$, $(1.60, 1.005)$, $(1.67, 1.005)$, $(1.80, 1.005)$, $(1.71, 0.97)$, and $(1.80, 0.97)$.

(ii) The region where a single critical point appears (upper side of figure 3). The leftward boundary between this single critical point domain and no critical point one is $E=E_{mb}=1$. The type of critical points in this domain is always the saddle type. Critical solutions of the spherical Bondi (1952) type for small L smoothly transit to the disk accretion type for large L.

(iii) The region where multiple critical points appear (central triangle part in figure 4). In this region, when E is smaller than unity (bound flow), there exist two critical points, whereas there are three for $E>1$ (unbound flow). In addition, above the double line (i.e., higher E and/or higher L) a critical solution which extends from infinity to the center passes through inner critical points, while it passes through outer ones below the double line (i.e., lower E and/or lower L) for $E>1$. The bifurcation points surrounding this domain are $(L, E, r_c)=(1.4047, 1.0087, 6.7)$, $(1.5151, E_{mb}, 4.3)$, $(L_{ms}, E_{ms}, 3)$, and $(L_{mb}, E_{mb}, 2)$, where $L_{mb}=2$.

The division of the L-E plane is qualitatively similar to that for the polytropic case (appendix 2), but quantitatively different from it.

In figure 5, the Mach numbers of solutions in various domains in figure 4 are shown as functions of r. Parameters are $(L, E)=(1.20, 1.04)$, $(1.50, 1.04)$, $(1.20, 1.005)$, $(1.46, 1.005)$, $(1.50, 1.005)$, $(1.52, 1.0005)$, $(1.60, 1.005)$, $(1.67, 1.005)$, $(1.80, 1.005)$, $(1.71, 0.97)$, and $(1.80, 0.97)$ from top-left to bottom-right.

When we fix the parameter E at a value between 1.0087 and E_{mb}, critical solutions for small L pass through outer critical points of the saddle type [spherical Bondi (1952) type accretion], while those for large L pass through inner points of the saddle type (disk-type accretion), as demonstrated in earlier investigations for the polytropic flow (Abramowicz and Zurek 1981; Abramowicz et al. 1986).

Similarly, when we fix the value of L between 1.4047 and L_{mb}, then critical solutions pass through outer critical points for small E and inner ones for large E. Then, it is emphasized that *the locations of critical points jump and the transonic solutions change drastically, if the values of parameters change so as to cross the double line in figure 4.* The bimodal behavior of transonic disk accretion of gas with angular momentum is thus extended in a general case.

5. Standing Shocks

Through standing shock waves, supersonically accreting steady flows can transit to subsonic ones which settle hydrostatically down the rigid surface of a central gravitating object. In the Newtonian case, such standing shocks associated with accretion or wind have been extensively studied (McCrea 1956; Holzer and Axford 1970). On the other hand, in the relativistic case discussed here, little has been done except for the spherical case (Blumenthal and Mathews 1976). The transition through standing shocks, however, is a serious problem in transonic (disk) accretion onto compact objects such as a neutron star and even a black hole. In this section, standing shocks are thus incorporated in the present transonic flow.

In the context of the present treatment under the spherical geometry, we cannot deal properly with such a standing shock in disk accreting flows. This is because the hydrostatic equilibrium in the vertical direction of the disk is not considered and hence the vertical expansion just behind the shock will not be taken into account (see Fukue 1983). Qualitative features, however, can be found under the limited treatment here as described below.

In order to derive the jump conditions, we must use the relativistic Rankine–Hugoniot relations (Thorne 1973). Considered here are shocks standing stationary

at the same positions in accreting flows, so the shock frame (a local Lorentz frame) coincides with the rest one. Moreover, it is unnecessary to consider the tangential component of the flow in the jump conditions. I further assume that the thickness of the flow does not change at the shock. Hence, the jump conditions become

$$n_1 u_1 = n_2 u_2 \,, \tag{17a}$$

$$(\varepsilon_1 + p_1) u_1^2 + p_1 = (\varepsilon_2 + p_2) u_2^2 + p_2 \,, \tag{17b}$$

$$(\varepsilon_1 + p_1) \gamma_1 u_1 = (\varepsilon_2 + p_2) \gamma_2 u_2 \,, \tag{17c}$$

where 1 denotes the front side of the shock and 2 the back side. The four velocity u and the Lorentz factor γ should be read as $u=\gamma v$ and $\gamma=(1-v^2)^{-1/2}$ in this section.

By adopting T and u as variables, equations (17a)–(17c) are reduced to

$$(f_p + f_e + 2kT)\gamma|_1 = (f_p + f_e + 2kT)\gamma|_2 \,, \tag{18a}$$

$$[2kT + (f_p + f_e + 2kT)u^2]/u|_1 = [2kT + (f_p + f_e + 2kT)u^2]/u|_2 \,. \tag{18b}$$

From these equations (18a) and (18b), we can calculate the postshock quantities from the preshock quantities given.

5.1. *Neutron Stars*

Let us first consider standing shocks in the disk accretion onto a neutron star which has a *rigid* surface. In this case, the subsonic flow inside the standing shock must connect smoothly to the boundary conditions at the star surface.

A typical example is shown in figure 6, where parameters are fixed as $E=1.005$ and $L=1.500$ as in figure 3a. Hence, the outer critical point is located at $r=27.67$

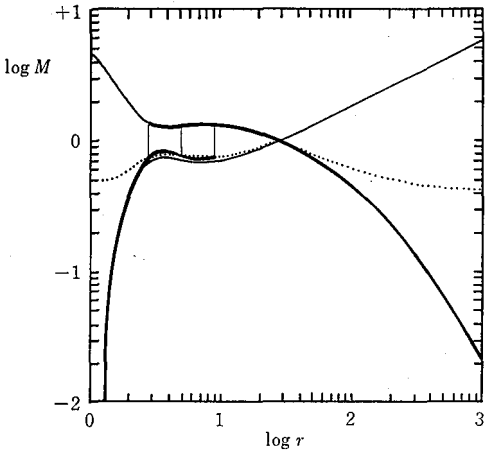

Fig. 6. The Mach number M of an example of solutions with standing shocks in the case of accretion onto a neutron star. Parameters are $(L, E)=(1.500, 1.005)$. The dotted curve denotes the locus of the Mach number just behind the shock. Thin vertical lines represent the positions of standing shocks for the conditions specified. The shocks can stand at three distinct locations for the same parameters and boundary conditions in this case.

and the effective adiabatic index there is 1.445. The radius r_* of the neutron star is assumed to be $2r_g$ and the temperature there is set as $kT/m_pc^2=0.03$ in this example.

In figure 6, the Mach number M is plotted as a function of r. The dotted curve denotes the locus of M at the postshock position. The supersonic solution jumps on this curve at the shock. The relevant parts of the solutions are denoted by thick curves. It is found that, *for the same parameters of the flow and for the same boundary conditions at the star surface, shocks can stand at three distinct positions in this case.* In the case of figure 6, the possible locations of standing shocks are ~ 9, ~ 5, and ~ 2.6.

This phenomenon may be associated with the multiplicity of critical points mentioned in section 3. Of these three locations of standing shocks, the outermost position is that of the usual type formed in the spherical flow. The intermediate position appears due to the effect of rotation (this is easily understood when we consider the Newtonian limit). Finally, the innermost position is related to the relativistic effect.

Which location of these shock positions does nature favor? Undoubtedly, a more detailed analysis is necessary, including the stability of standing shock waves. This is out of the scope of this paper.

5.2. *Black Holes*

In usual situations, it seems to be difficult to imagine standing shocks in a transonic accretion onto a black hole which has *no rigid* surface. In the present case, however, the multiplicity of critical points enables standing shocks in such a transonic flow onto (into?) a black hole.

An example is displayed in figure 7, where parameters are $E=1.005$ and $L=1.513$, and therefore $r_c=27.3$ and $\Gamma_c=1.445$.

In figure 7, the dotted curve also denotes the locus of the Mach number just behind the shock. The supersonically accreting flow which has passed through the *outer* critical point of the saddle type becomes subsonic at the standing shock. Then it is

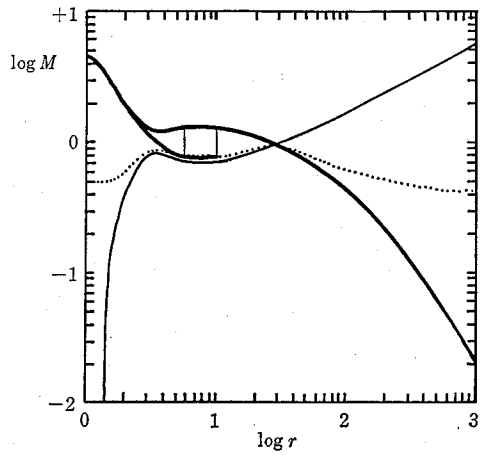

Fig. 7. Same as figure 6 but for a black hole. $(L, E)=(1.513, 1.005)$. In addition to the transonic solution without a shock, there exist two with standing shocks at different radii.

again accelerated to be supersonic at the *inner* critical point and eventually falls into the hole. In the case of figure 7, it is possible for standing shocks to exist at two different places, $r=5.6$ and 10. This is also due to reasons similar to those discussed in the previous subsection. In addition, it is of course possible to have a transonic solution without a shock.

I notice that the standing shock which appeared in the accretion onto a black hole for the present case is different from that discussed by Chang and Ostriker (1985) in the spherical accretion where the nonadiabatic effect is included.

6. An Application

Transonic flows (with standing shocks) will be established in various situations as already suggested in the introduction (figure 1). That is, in the case of disk accretion of unbound gas, inside the inner edge of a geometrically thin accretion disk, inside the cusp of an accretion torus, etc.

In this section, I shall apply transonic disk accretions discussed in the previous sections to low-mass binary X-ray sources, which have been extensively observed by the X-ray astronomy satellite Tenma (e.g., Mitsuda et al. 1984).

Energy spectra from these low-mass binaries are believed to consist of two distinct components: a nonvarying soft component showing a blackbody spectrum of ~ 1 keV, and a hard component showing a ~ 2-keV blackbody and varying in intensity. This is interpreted as follows; i.e., the soft component originates mainly from the inner region of a geometrically thin and optically thick accretion disk around a compact object, while the hard one comes from the surface layer formed by the accreting material on the neutron star. Furthermore, the thin accretion disk is supposed to extend very close to the neutron star (figure 1b). However, the separation between the soft and hard components suggests that there still exists some gap—an optically thin region—between the inner edge of the accretion disk and the star surface.

Tenma has also discovered absorption lines at the energy level ~ 4.1 keV in the spectra from X-ray bursters X1636−536 (Waki et al. 1984). These lines are identified with the 6.7-keV resonance line of the helium-like iron ion which is redshifted by the strong gravitational field near the surface of the neutron star. The resultant radius of the neutron star is about $1.6r_g$. Although there are several arguments (e.g., Fujimoto 1985), the radius of the neutron star in X1636−536 may lie between $1.6r_g$–$2.4r_g$; i.e., *smaller than* r_{ms} in any case.

These facts lead us to the following picture; the radius r_* of a neutron star without rotation and magnetic field is generally smaller than the marginally stable radius r_{ms} of the star. Hence, inside r_{ms}, the accreting material which forms a geometrically thin accretion disk outside r_{ms} infalls transonically onto the surface of the neutron star. In this region between r_{ms} and r_*, gas is remarkably rarefied by the rapid infall. In figure 8, these situations are schematically shown.

Now let us apply the present model to such a flow inside r_{ms} in low-mass binary X-ray sources. In order to specify the flow, two boundary conditions are necessary. The specific angular momentum around r_{ms} is very close to L_{ms}; so I first set $L=L_{ms}$ in the model. From observations (Mitsuda et al. 1984), the temperature of the inner

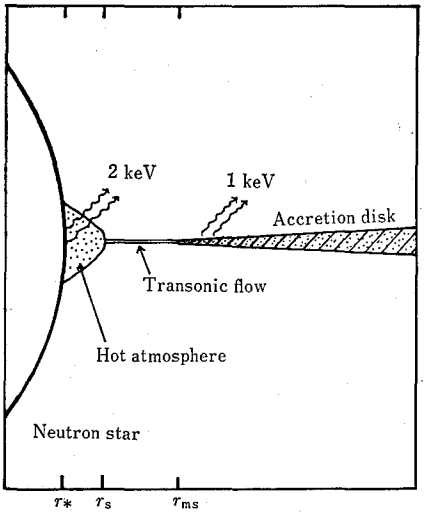

Fig. 8. A possible schematic view around a neutron star in low-mass binary X-ray sources.

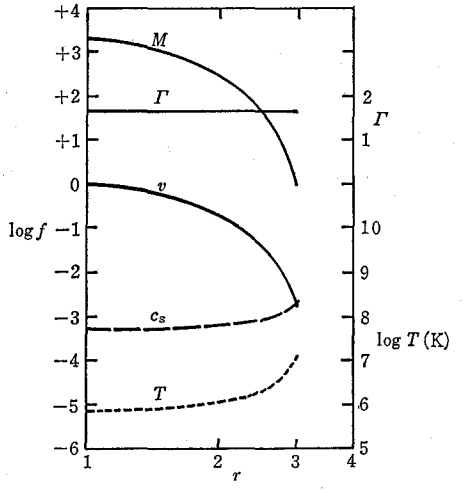

Fig. 9. Cold transonic flow inside the inner edge of a geometrically thin accretion disk in low-mass binary X-ray sources. Parameters are $L=L_{ms}$ and $T=1.2\times10^7$ K at r_{ms}. Thus $E=0.942816$, $r_c=2.9828$, and $\Gamma_c=1.6650$. It is emphasized that the temperature decreases inward because of the rapid infall.

region of the accretion disk is ~ 1 keV and thereby I have next set the temperature of the transonic flow just inside r_{ms} 1.2×10^7 K at r_{ms}. The results are shown in figure 9.

In actual calculations, I have expanded equations (15), (9), and (14) around the critical point to obtain several quantities, because the flow is too cold to solve directly the critical condition (15). For example, the critical point is located at $r_c=2.9828$, very close to r_{ms}, and the specific energy is $E=0.942816$ which is a bit larger than $E_{ms}=(8/9)^{1/2}$. Moreover, the adiabatic index at the critical point is $\Gamma_c=1.6650\sim5/3$.

As seen from figure 9, the infalling velocity increases rapidly inward due to the

general relativistic effect. As a result, *the temperature decreases inward against the geometrical contraction*; i.e., adiabatic expansion takes place in this case in spite of the fact that the relevant flow is accretion. Furthermore, the flow becomes highly supersonic here. In the case of an accretion onto a black hole from the inner edge of geometrically thin accretion disks, the solution displayed in figure 9 may extend to the horizon; near the horizon of a black hole the flow is almost free fall and isothermal [see Bernoulli equation (9)].

However, when the central compact star is a neutron star as considered here, shock waves should stand in the accretion flow and through it the supersonic flow turns to the subsonic one extending to the neutron star surface. Just inside the shock, the gas will be significantly heated up to the level of the deep effective potential. In the case of figure 9, the temperature just inside the shock becomes about 100 keV, when the shock is located at $r_s=2.5r_g$ and about 10^3 keV for $r_s=2r_g$. The flow inside the shock will thus form a very hot hydrostatic atmosphere rotating around a neutron star and eventually connecting to the star surface through the cool surface layer of ~ 2 keV (see figure 8). This possible hot atmosphere can Comptonize the blackbody photons of ~ 2 keV from the surface of the neutron star.

These pictures are the natural consequence when the radius of the neutron star is smaller than the inner edge of accretion disks.

7. Concluding Remarks

In this paper, the transonic disk accretion onto compact objects is extensively examined under a full relativistic treatment with the rigorous equations of state. The main results obtained are summarized as follows:

1. Multiplicity of critical points has been also found in the present case similar to the polytropic flow (figures 2 and A2). This is due to the effects of rotation and relativity. The parameter range allowing multiple critical points was obtained quantitatively. In addition, the types of critical points are the saddle type or the center type as long as the adiabatic flow is relevant.

2. Critical solutions are classified on the *L-E* parameter plane (figures 4 and A3). The plane is divided into three regions via the number of critical points. The bimodal behavior between the nearly spherical flow and the disk flow suggested in the previous studies is generalized on this plane.

3. The equations of state adopted quantitatively modify the solutions in comparison with those of the polytropic case. Furthermore, the adiabatic index is no longer a parameter in the present case (figure A1).

4. Standing shock waves have been taken into considerations (figures 6 and 7) for the first time. It was found that shocks can stand at several radii for the same parameters and boundary conditions. Moreover, shocks stand in the transonic flow onto not only a neutron star but also a black hole. These are also due to the effects of rotation and relativity.

5. Applications were made to the case of low-mass binary X-ray sources (figures 8 and 9). In these objects, a very cold transonic flow may be established inside the inner edge of the geometrically thin accretion disk. It further becomes the hot atmos-

phere surrounding a neutron star via standing shocks. This hot plasma can Comptonize the emission from the surface layer of the neutron star.

At the present stage, instead of solving exactly the hydrostatic balance in the vertical direction of the disk, I have assumed a cross-sectional area of the disk flow for simplicity. Hence, the effect of vertical expansion, which cools the shock-heated gas, just behind the shock is not taken into account (cf. Fukue 1983). There are further open questions; which position of the shocks we should select; whether the standing shocks are stable or not; how the subsonic flow inside the shock eventually settles down on the surface of compact stars. These as well as the cases of nonadiabaticity and two temperatures for the accreting gas are left as future work.

This work was supported in part by a Grant-in-Aid for the Scientific Research of the Ministry of Education, Science, and Culture (61740141).

Appendix 1. Adiabatic Sound Speed and Effective Adiabatic Index

In the present analysis, I have used the rigorous equations of state derived from the relativistic Maxwell–Boltzmann distribution of gas (Cox and Giuli 1968), unlike previous studies adopting the polytropic relation. For convenience of the reader, I here summarize several relations: the equations of state, the adiabatic sound speed, and the effective adiabatic index (cf. Fukue 1986).

For the a-th species of rest mass m_a, the pressure p_a and the internal energy density ε_a are respectively expressed in terms of the number density n_a and of the temperature T_a as

$$p_a=n_a k T_a\ , \tag{A1}$$

$$\varepsilon_a=n_a f_a(T_a)\ , \tag{A2}$$

where

$$f_a(T_a)=m_a c^2\left[\frac{3kT_a}{m_a c^2}+\frac{K_1(m_a c^2/kT_a)}{K_2(m_a c^2/kT_a)}\right], \tag{A3}$$

and k is the Boltzmann constant. Here K_n's are the modified Bessel functions of the second kind of order n. For electron-proton gas with the same temperature T, equations (A1) and (A2) are reduced to equations (7) and (8) in the text.

The adiabatic sound speed is defined by (Fukue 1986)

$$c_s^2\equiv\Gamma P/(\varepsilon+p)\ , \tag{A4}$$

where Γ is the effective adiabatic index:

$$\Gamma=[1+p/\textstyle\sum Tn_a f_a'(T_a)]\ , \tag{A5}$$

the prime denoting the differentiation with respect to T. For electron-proton gas, equations (A4) and (A5) are reduced respectively to

$$c_s^2=\Gamma\frac{2kT}{f_p+f_e+2kT}\ , \tag{A6}$$

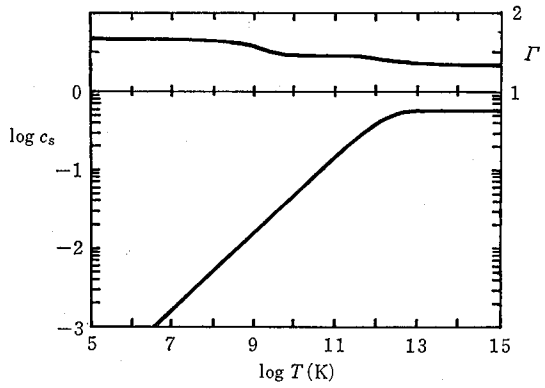

Fig. A1. The adiabatic sound speed c_s and the effective adiabatic index Γ versus T.

$$\Gamma=[1+2k/(f_p'+f_e')]\,. \tag{A7}$$

These adiabatic sound speed and adiabatic index are shown in figure A1 as functions of T.

It is worthwhile to note that the value of Γ is nearly constant in three regimes: that is, 5/3 at $kT<m_ec^2$ where both electrons and protons are nonrelativistic, ~ 1.44 at $m_ec^2<kT<m_pc^2$ where electrons become relativistic, while protons remain nonrelativistic, and 4/3 at $kT>m_pc^2$ where both are relativistic.

Appendix 2. Polytropic Disk Accretion

In the investigations so far, the polytropic relation has been adopted for simplicity [Lu (1985) and references therein]. In this appendix, I summarize the results of such a polytropic flow in order to compare them with the present results.

For the polytropic flow, we adopt the polytropic relation:

$$p/n^\Gamma=\text{constant}\,, \tag{A8}$$

instead of the equations of state (7) and (8). Hence the Bernoulli equation (9) is replaced by

$$\frac{\varepsilon+p}{n}u_0=\text{constant}\,. \tag{A9}$$

Moreover, although the wind equation for the polytropic flow has the same form as equation (12), the sound speed (14) should be read as, with the help of thermodynamic equality and the Bernoulli equation,

$$c_s^2=\Gamma p/(\varepsilon+p)=\begin{cases}(\Gamma-1)(1-u_0/E) & \text{for } \Gamma\neq 1\,,\\ u_0/E' & \text{for } \Gamma=1\,,\end{cases} \tag{A10}$$

where E and E' are constants.

I emphasize that *the index Γ must be given as a free parameter in the polytropic flow, whereas it is determined uniquely as a function of temperature in the present case*

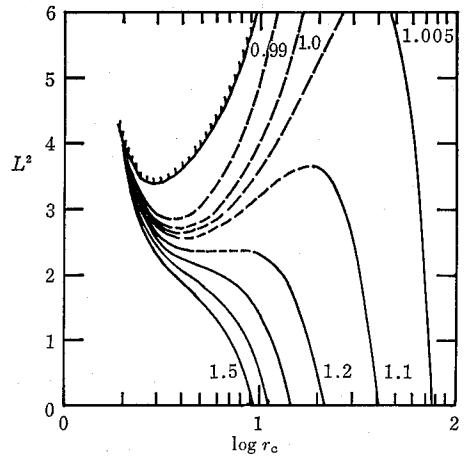

Fig. A2. The relations among L, E, and r_c in the polytropic case (Lu 1985). The parameters are $N=2$ and $\Gamma=4/3$. The hatched region is forbidden because $v^2|_c<0$. See also figure 2.

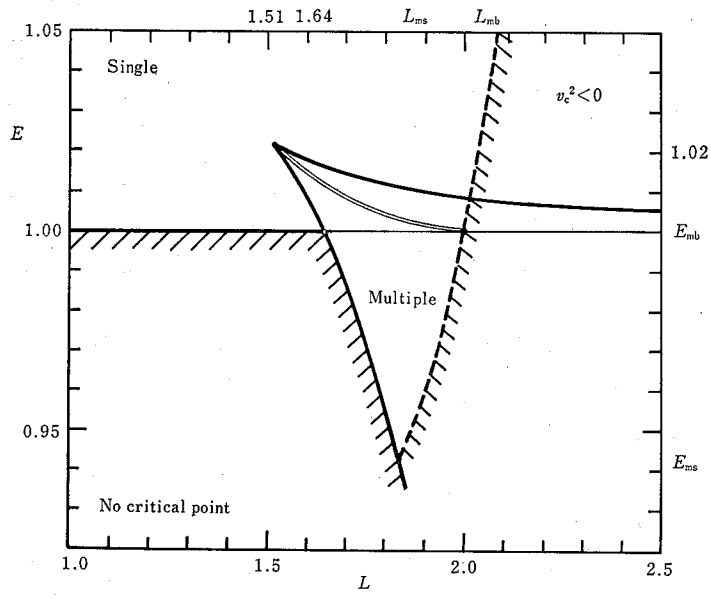

Fig. A3. Classification diagram in the polytropic case (see also figure 4). The bifurcation points are $(L, E, r_c)=(1.5165, 1.0215, 5.9)$, $(1.6422, E_{mb}, 3.8)$, $(L_{ms}, E_{ms}, 3)$, and $(L_{mb}, E_{mb}, 2)$.

[*equation* (*A7*)].

The relations among L, E, and r_c obtained in the polytropic case (Lu 1985) are qualitatively similar to those in figure 2 but quantitatively different from it. They are reproduced in figure A2. Parameters given are $N=2$ and $\Gamma=4/3$. There are three critical points for $1<E<1.02$ in the polytropic case, while there are three for $1<E<1.009$ in the case examined in the text. This is because the effective index is larger

than 4/3 in the text.

Critical solutions are also classified on the L-E parameter plane in the polytropic case (figure A3). The parameters are also $N=2$ and $\Gamma=4/3$ (see also figure 4).

The features of transonic solutions and standing shocks in the polytropic case are qualitatively similar to those in the case where the rigorous equations of state are adopted.

References

Abramowicz, M. A., Blaes, O. M., and Lu, J. 1986, in *Structure and Evolution of Active Galactic Nuclei*, ed. G. Giuricin, F. Mardirossian, M. Mezzetti, and M. Ramella (D. Reidel, Dordrecht), p. 113.

Abramowicz, M. A., and Zurek, W. H. 1981, *Astrophys. J.*, **246**, 314.

Blumenthal, G. R., and Mathews, W. G. 1976, *Astrophys. J.*, **203**, 714.

Bondi, H. 1952, *Monthly Notices Roy. Astron. Soc.*, **112**, 195.

Chang, K. M., and Ostriker, J. P. 1985, *Astrophys. J.*, **288**, 428.

Cox, J. P., and Giuli, R. T. 1968, *Principles of Stellar Structure, Vol. 2* (Gordon and Breach, New York), chap. 24.

Fujimoto, M. Y. 1985, *Astrophys. J. Letters*, **293**, L19.

Fukue, J. 1983, *Publ. Astron. Soc. Japan*, **35**, 355.

Fukue, J. 1986, *Publ. Astron. Soc. Japan*, **38**, 167.

Henriksen, R. N., and Heaton, K. C. 1975, *Monthly Notices Roy. Astron. Soc.*, **171**, 27.

Holzer, T. E., and Axford, W. I. 1970, *Ann. Rev. Astron. Astrophys.*, **8**, 31.

Kozłowsky, M., Jaroszyński, M., and Abramowicz, M. A. 1978, *Astron. Astrophys.*, **63**, 209.

Liang, E. P. T., and Thompson, K. A. 1980, *Astrophys. J.*, **240**, 271.

Limber, D. N. 1967, *Astrophys. J.*, **148**, 141.

Loska, Z. 1982, *Acta Astron.*, **32**, 13.

Lu, J. F. 1985, *Astron. Astrophys.*, **148**, 176.

Matsumoto, R., Kato, S., Fukue, J., and Okazaki, A. T., 1984, *Publ. Astron. Soc. Japan*, **36**, 71.

McCrea, W. H. 1956, *Astrophys. J.*, **124**, 461.

Mitsuda, K., Inoue, H., Koyama, K., Makishima, K., Matsuoka, M., Ogawara, Y., Shibazaki, N., Suzuki, K., Tanaka, Y., and Hirano, T. 1984, *Publ. Astron. Soc. Japan*, **36**, 741.

Muchotrzeb, B. 1983, *Acta Astron.*, **33**, 79.

Novikov, I. D., and Thorne, K. S. 1973, in *Black Holes*, ed. C. DeWitt and B. S. DeWitt (Gordon and Breach, New York), p. 343.

Rees, M. J., Begelman, M. C., Blandford, R. D., and Phinney, E. S. 1982, *Nature*, **295**, 17.

Shakura, N. I., and Sunyaev, R. A. 1973, *Astron. Astrophys.*, **24**, 337.

Thorne, K. S. 1973, *Astrophys. J.*, **179**, 897.

Waki, I., Inoue, H., Koyama, K., Matsuoka, M., Murakami, T., Ogawara, Y., Ohashi, T., Tanaka, Y., Hayakawa, S., Tawara, Y., Miyamoto, S., Tsunemi, H., and Kondo, I. 1984, *Publ. Astron. Soc. Japan*, **36**, 819.